Corrected 30 March 2020. See full text.

PHYSICS

Twisted bulk-boundary correspondence of fragile topology

Zhi-Da Song[1], Luis Elcoro[2], B. Andrei Bernevig[1,3,4]*

A topological insulator reveals its nontrivial bulk through the presence of gapless edge states: This is called the bulk-boundary correspondence. However, the recent discovery of "fragile" topological states with no gapless edges casts doubt on this concept. We propose a generalization of the bulk-boundary correspondence: a transformation under which the gap between the fragile phase and other bands must close. We derive specific twisted boundary conditions (TBCs) that can detect all the two-dimensional eigenvalue fragile phases. We develop the concept of real-space invariants, local good quantum numbers in real space, which fully characterize these phases and determine the number of gap closings under the TBCs. Realizations of the TBCs in metamaterials are proposed, thereby providing a route to their experimental verification.

Topological insulators are materials that conduct no electricity in the bulk but that allow perfect passing of the current through their edges. This is the basic concept of the bulk-boundary correspondence: A topological bulk is accompanied by a gapless edge. New theories (*1*–*4*) have developed systematic methods for searching topological materials (*5*–*7*). This led to the discovery of higher-order topological insulators (HOTIs) (*8*–*11*) and fragile topological states (*12*–*16*), the latter being predicted (*17*, *18*) to exist in the newly discovered twisted bilayer graphene (*19*). The fragile phases generally do not exhibit gapless edges, thereby violating the bulk-boundary correspondence.

We show that fragile phases exhibit a new type of bulk-boundary correspondence with gapless edges under "twisted" boundary conditions (TBCs). TBCs were introduced (*20*) to prove the quantization of Hall conductance. On a torus, a particle under U(1) TBCs gains a phase $e^{i\theta_{x,y}}$ whenever it undergoes a period in the x/y direction. This phase was generalized to a complex number $\lambda = re^{i\theta}(0 \le r \le 1)$ (*21*) for a trivial state with two pairs of helical edge states, with unclear results. We consider a slow deformation of the boundary condition controlled by a single parameter, λ. If the fragile phase, determined by eigenvalues, can be written as a difference of a trivial atomic insulator and an obstructed atomic insulator (with electron center away from atoms), the energy gap between the fragile bands and other bands must close as we tune λ on a particular path.

We develop a real-space invariant (RSI) (*22*, *23*), to classify eigenvalue fragile phases (EFPs) and their spectral flow under TBCs. RSIs are local quantum numbers protected by point group (PG) symmetries. With translation symmetry, they can be calculated from symmetry eigenvalues of the band structure. Under a specific evolution of the boundary condition, where the symmetry of some lattice (Wyckoff) position is preserved, the system goes through a gauge transformation, which does not commute with the symmetry operators. The symmetry eigenvalues and the RSIs at this Wyckoff position also go through a transformation: If the RSIs change, a gap closing happens during the process. We find that EFPs always have nonzero RSIs: Therefore, TBCs generally detect fragile topology. A real-space approach has also been useful for (non-) interacting (*24*–*26*) strong crystalline topological states. We obtain the full classification of RSIs for all two-dimensional (2D) PGs with and without spin-orbit coupling (SOC) and/or time-reversal symmetry (TRS), and we derive their momentum space formulae [table S5 (*27*)]. For each 2D PG, we introduce a set of TBCs to detect the RSIs (*27*). Criteria for stable and fragile phases are written in terms of RSIs [table S6 (*27*)] and exemplified on a spinless model.

The symmetry property of bands is fully described by its decompositions into irreducible representations (irreps) of little groups at momenta in the first Brillouin zone (BZ). Topological quantum chemistry (*1*) and related theories (*3*, *4*) provide a general framework to diagnose whether a band structure is topological from the irreps. If the irreps of a band structure are the same as those of a band representation (BR), which is a space group representation formed by decoupled symmetric atomic orbitals, representing atomic insulators, then the band structure is consistent with topologically trivial state; otherwise, the band structure must be topological. Generators of BRs are called elementary BRs (EBRs) (*1*). The EBRs in all space groups are available on the Bilbao Crystallographic Server (BCS) (*1*, *28*). We will demonstrate this principle using a tight-binding model in the following.

There are two distinct categories of topological band structures. If a topological band structure becomes a BR (in terms of irreps) after being coupled to a topologically trivial band, the band structure has at least a fragile topology. We refer to such a phase as an EFP. An EFP may also have a stable topology undiagnosed from symmetry eigenvalues (*14*, *29*). If the band structure remains inconsistent with a BR after being coupled to any topologically trivial bands, the band structure has a stable topology. Further discussions about the classifications of topological and nontopological bands can be found in (*27*).

We build a spinless model whose bands split into an EFP branch and an obstructed atomic insulator branch. Consider a C_4 symmetric square lattice (wallpaper group $p4$). Its BZ has three maximal momenta $\Gamma(0,0)$, $M(\pi,\pi)$, and $X(\pi,0)$. The little group of Γ and M is PG 4, and the little group of X is PG 2, with irreps tabulated in Table 1. The irreps form co-irreps when we impose TRS. We tabulate all the EBRs of $p4$ with TRS in Fig. 1. Here we consider the EFP $2\Gamma_1 + 2M_2 + 2X_1$, a state of two bands where each band forms the irreps Γ_1, M_2, X_1 at Γ, M, X. These bands are topological: They cannot decompose into a sum of EBRs. The EFP is (necessarily) a difference of EBRs as $2(A)_b\uparrow G \oplus ({}^1E^2E)_b\uparrow G \ominus ({}^1E^2E)_a\uparrow G$.

Consider a four-band model of two s (s_1 and s_2), one p_x, and one p_y orbitals at the b position (Fig. 2A). Per Table 1, $s_{1,2}$ orbitals (irrep A) induce the BR $2(A)_b\uparrow G = 2\Gamma_1 + 2M_2 + 2X_2$; $p_{x,y}$ orbitals (irrep ${}^1E^2E$) induce the EBR $({}^1E^2E)_b\uparrow G = \Gamma_3\Gamma_4 + M_3M_4 + 2X_1$. Let the $p_{x,y}$ orbitals have a higher energy than the $s_{1,2}$ orbitals. We band invert at the X point such that the upper two bands' irreps become $\Gamma_3\Gamma_4 + M_3M_4 + 2X_2 = ({}^1E^2E)_a\uparrow G$ (an EBR), and the lower two bands have the EFP irreps $2\Gamma_1 + 2M_2 + 2X_1$. Because the upper band forms

Table 1. Character tables of irreps of PGs 2 and 4. First column: BCS notations (*28*) of the PG irreps. Second column: notations of momentum space irreps at X, Γ, and M for wallpaper group $p4$. The third column is the atomic orbitals forming the corresponding irreps. In the presence of TRS, the two irreps ${}^1E$ (Γ_3, M_3) and ${}^2E$ (Γ_4, M_4) of PG 4 form the co-irrep ${}^1E^2E$ ($\Gamma_3\Gamma_4$, M_3M_4).

PG 2			1	2	PG 4			1	4^+	2	4^-
A	X_1	s	1	1	A	Γ_1, M_1	s	1	1	1	1
B	X_2	p_x	1	−1	B	Γ_2, M_2	d_{xy}	1	−1	1	−1
					${}^1E$	Γ_3, M_3	$p_x + ip_y$	1	$-i$	−1	i
					${}^2E$	Γ_4, M_4		1	i	−1	i

[1]Department of Physics, Princeton University Princeton, NJ 08544, USA. [2]Department of Condensed Matter Physics, University of the Basque Country UPV/EHU, Apartado 644, 48080 Bilbao, Spain. [3]Physics Department, Freie Universitat Berlin Arnimallee 14, 14195 Berlin, Germany. [4]Max Planck Institute of Microstructure Physics, 06120 Halle, Germany.
*Corresponding author. Email: bernevig@princeton.edu

Corrected 30 March 2020. See full text.

an EBR at the empty Wyckoff position, where no atom exists, it forms an obstructed atomic insulator band. The model, in the basis (p_x, p_y, s_1, s_2), is (*27*)

$$H(\mathbf{k}) = \tau_z\sigma_0\Big(E + 2t_1\cos(k_x + k_y) + 2t_1\cos(k_x - k_y)\Big) + \tau_y\sigma_z t_2\sin(k_x) + \tau_y\sigma_x t_2\sin(k_y) \quad (1)$$

E ($-E$) is the onsite energy for the $p_{x,y}$ ($s_{1,2}$) orbitals, t_1 band inverts at X, and t_2 guarantees a full gap between the upper and lower two bands. We introduce $\Delta H(\mathbf{k})$ (*27*) to break two accidental symmetries, M_z ($z \to -z$) $= \tau_z\sigma_y$, chiral $\tau_x\sigma_0$. The band structure of $H(\mathbf{k}) + \Delta H(\mathbf{k})$ is plotted in Fig. 2B.

We construct a finite-size (30 × 30) TRS Hamiltonian with C_4 rotation symmetry preserved at the coordinate origin on the *a* site (Fig. 2C). The spectrum consists of 1798 occupied states, 4 degenerate partially occupied levels at the Fermi level, and 1798 empty levels; they form the representations $450A\oplus 450B\oplus 449(^1E^2E)$, $A\oplus B\oplus{}^1E^2E$, and $449A\oplus 449B\oplus 450(^1E^2E)$, respectively. The partially occupied states are corner states, or the "filling anomaly" of fragile topology (Fig. 2C). The gap between the four partially occupied levels and the occupied or empty levels is about 0.3/0.01, as $\Delta H(\mathbf{k})$ breaks the accidental chiral symmetry. Every four states forming the irreps $A\oplus B\oplus{}^1E^2E$ can be recombined as $|1\rangle = (|A\rangle + |B\rangle + |^1E\rangle + |^2E\rangle)/2$, $|2\rangle = (|A\rangle - |B\rangle - i|^1E\rangle + i|^2E\rangle)/2$, $|3\rangle = (|A\rangle + |B\rangle - |^1E\rangle - |^2E\rangle)/2$, and $|4\rangle = (|A\rangle - |B\rangle + i|^1E\rangle - i|^2E\rangle)/2$, which transform to each other under the C_4 rotation and have Wannier centers away from the C_4 center: We hence move the occupied and empty states, both of which form the representation $449A\oplus 449B\oplus 449(^1E^2E)$, away from the C_4 center. We are left with two occupied states, $A\oplus B$, and two empty states, $(^1E^2E)$, at the C_4 center. These four states form a level crossing under TBC evolution.

We divide (Fig. 2C) the system into four parts (μ = I, II, III, IV), which transform into each other under C_4. We introduce the TBC by multiplying the hoppings between different parts by specific factors such that the twisted and original Hamiltonians are equivalent up to a gauge transformation. Specifically, the multiplication factors on hoppings from μth part to $(\mu+1)$th part, from μth part to $(\mu+2)$th part, from μth part to $(\mu-1)$th part are i, -1, $-i$. The twisted and untwisted Hamiltonians $\hat{H}(i), \hat{H}(1)$ satisfy

$$\langle\mu,\alpha|\hat{H}(i)|\nu,\beta\rangle \equiv (i)^{\nu-\mu}\langle\mu,\alpha|\hat{H}(1)|\nu,\beta\rangle \quad (2)$$

$|\mu,\alpha\rangle$ is the αth orbital in the μth part, and $H(\lambda)$ is the Hamiltonian with multiplier λ. We introduce the twisted basis $\hat{V}|\mu,\alpha\rangle = (-i)^{\mu-1}|\mu,\alpha\rangle$. The elements of $\hat{H}(i)$ on the twisted basis equal those of $\hat{H}(1)$ on the untwisted basis: $\langle\mu,\alpha|\hat{V}^\dagger\hat{H}(i)\hat{V}|\nu,\beta\rangle = \langle\mu,\alpha|\hat{H}(1)|\nu,\beta\rangle$. C_4 transforms the μth part into the $(\mu+1)$th part: The twisting phases of $|\mu,\alpha\rangle$ and $\hat{C}_4|\mu,\alpha\rangle$ under $\hat{V}$ are $(-i)^{(\mu-1)}$ and $(-i)^\mu$, implying $\hat{V}\hat{C}_4 = -i\hat{C}_4\hat{V}$. If $|\psi\rangle$ is an eigenstate of $\hat{H}(1)$ with C_4 eigenvalue ξ, then $\hat{V}|\psi\rangle$ will be an eigenstate of $\hat{H}(i) = \hat{V}\hat{H}(1)\hat{V}^\dagger$ of equal energy but different C_4 eigenvalue $i\xi$. The irreps A, B, ^1E, ^2E become ^2E, ^1E, A, B under the gauge transformation (Table 1). Therefore, two of the irreps $A\oplus B$ in the occupied states interchange with two of the irreps $^1E\oplus{}^2E$ in the empty states after the gauge transformation; all other irreps,

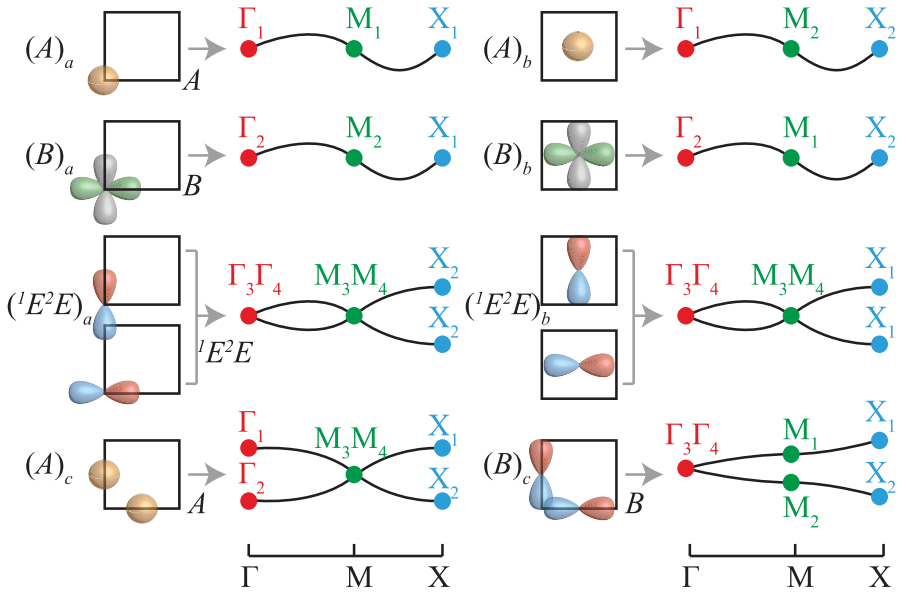

Fig. 1. EBRs of wallpaper group *p4* without SOC with TRS. [See BCS (*1*, *2*, *28*)]. The square represents the unit cell. *a* (0, 0), *b* $(\frac{1}{2},\frac{1}{2})$, *c* $(0,\frac{1}{2})$, $(\frac{1}{2},0)$ are maximal Wyckoff positions. The yellow, red and blue, and green and gray orbitals represent the *s*, $p_{x,y}$, and $d_{x^2-y^2}$ orbitals, respectively.

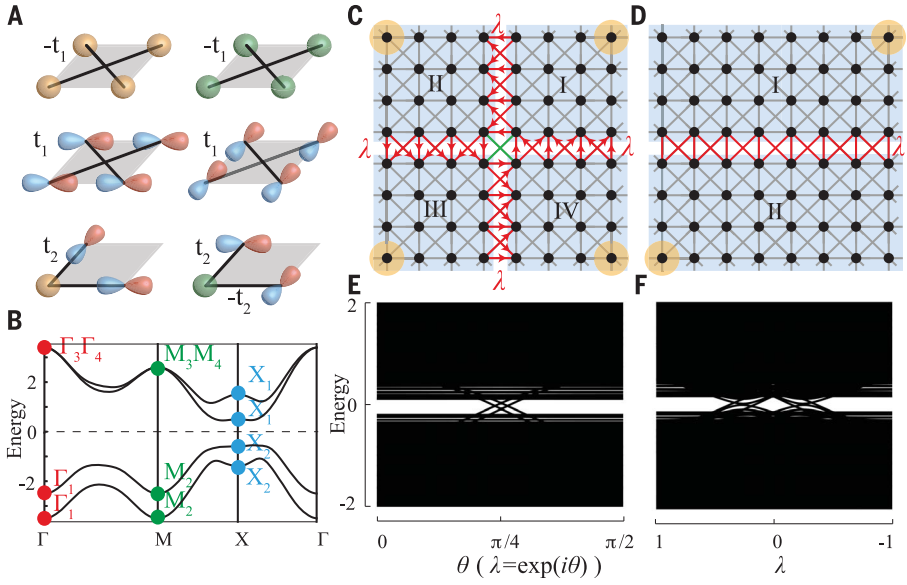

Fig. 2. Spectral flow of fragile phase under TBCs. (**A**) Fragile phase model (wallpaper group *p4* with TRS). The yellow, green, and red and blue orbitals are the two s and the $p_{x,y}$ orbitals. The gray parallelogram is the unit cell, and black lines are the hoppings. (**B**) Band structure of the fragile phase. (**C**) The C_4-symmetric TBCs of a finite size system. Black dots are the atoms; bonds are hoppings; four yellow circles are corner states of the fragile state. Four shaded regions (μ = I, II, III, IV) transform to each other under C_4 action. Hoppings from the μth part to the $(\mu+1)$th part (red bonds), from the μth part to the $(\mu+2)$th part (green bonds), and from the μth part to the $(\mu-1)$th part (red bonds) are multiplied by a complex λ/real $\mathrm{Re}(\lambda^2)$/complex λ^*. (**D**) The C_2 and TRS symmetric TBCs. The two shaded regions (μ = I, II) transform to each other under C_2 rotation. The hoppings between I, II (red bonds) are multiplied by a real number λ. (**E**) Spectral flow under C_4-symmetric TBC. (**F**) Spectral flow under C_2 and TRS symmetric TBCs.

($449A \oplus 449B \oplus 449(^1E) \oplus 449(^2E)$), remain unchanged. We generalize the C_4 symmetric TBC:

$$\langle \mu, \alpha|\hat{H}(\lambda)|\nu, \beta\rangle = \begin{cases} \langle \mu, \alpha|\hat{H}(1)|\nu, \beta\rangle, & \nu = \mu \\ \lambda\langle \mu, \alpha|\hat{H}(1)|\nu, \beta\rangle, & \nu = \mu + 1 \mod 4 \\ \lambda^*\langle \mu, \alpha|\hat{H}(1)|\nu, \beta\rangle, & \nu = \mu - 1 \mod 4 \\ \mathrm{Re}(\lambda^2)\langle \mu, \alpha|\hat{H}(1)|\nu, \beta\rangle, & \nu = \mu + 2 \mod 4 \end{cases} \quad (3)$$

$\mathrm{Re}(\lambda^2)$ is the real part of the complex λ^2. The factor between the μth and $(\mu + 2)$th part is real owing to C_2 (*27*). Equation 2 is the $\lambda = i$ case of Eq. 3. Under continuous tuning of λ from 1 to i, two occupied irreps $A \oplus B$ interchange with two empty irreps $^1E \oplus ^2E$. Their level crossings are protected by C_4 symmetry (Fig. 2E) [see (*27*) for other C_4 paths].

Now we consider C_4-breaking but C_2- and TRS-preserving TBCs. Divide the system into two parts (I,II), transforming into each other under C_2 (Fig. 2D), and multiply all hoppings between orbitals in part I and II by a real λ. The gauge transformation relating the twisted and untwisted Hamiltonians anticommutes with C_2: $\{\hat{V}, \hat{C}_2\} = 0$. $\hat{V}$ transforms between eigenstates of $\hat{H}(1)$, $\hat{H}(-1)$ with equal energy but opposite C_2 eigenvalue. Under a continuous tuning of λ from 1 to -1, the two final occupied (empty) states must have the C_2 eigenvalue -1 (1). This inconsistency implies C_2-protected gap closing, as shown in Fig. 2F. The unitary transformation relating $H(-1)$ to $H(1)$ also maps $H(-\lambda)$ to $H(\lambda)$, and the gap must close as λ changes from 1 to 0. In (*27*), we generalize the TBCs to all the 2D PGs. The gapless states under TBCs are the experimental consequences of the fragile states.

We introduce the RSI as an exhaustive description of the local states, pinned at the C_4 center, that undergo gap closing under TBCs. The Wannier centers of occupied states of a Hamiltonian can adiabatically move if their displacements preserve symmetry. Orbitals away from a symmetry center can move on it and form an induced representation of the site-symmetry group at the center. Conversely, orbitals at a symmetry center can move away from it symmetrically if and only if they form a representation induced from the site-symmetry groups away from the center. The RSIs are (*27*) linear invariant—upon such induction processes—functions of irrep multiplicities. For the PG 4 with TRS, we assume a linear-form RSI of the occupied levels $\delta = c_1 m(A) + c_2 m(B) + c_3 m(^1E^2E)$. The induced representation at the C_4 center from four states at C_4-related positions away from the center is $A \oplus B \oplus ^1E^2E$ (*27*). After the induction process, the irrep multiplicities at the C_4 center change as $m(A) \to m(A) + 1$, $m(B) \to m(B) + 1$, $m(^1E^2E) \to m(^1E^2E) + 1$. The two linear combinations of irrep multiplicities that remain invariant are

$$\delta_1 = m(^1E^2E) - m(A), \quad \delta_2 = m(B) - m(A) \quad (4)$$

In our model, the occupied states that can be moved away from the C_4 center form the representation $449A \oplus 449B \oplus 449(^1E^2E)$ and have vanishing RSIs. The states pinned at the C_4 center form $A \oplus B$ with RSIs $\delta_1 = -1, \delta = 0$. If an RSI is nonzero, spectral flow exists upon a particular TBC (*27*). We calculate all the RSIs in all 2D PGs with and without SOC or TRS [table S4 (*27*)]. The groups formed by RSIs are shown in Table 2. PG 4 with TRS has two integer-valued RSIs: The RSI group is $\mathbb{Z}^2$. Most RSIs are $\mathbb{Z}$-type; some groups with SOC and TRS have $\mathbb{Z}_2$-type RSIs, the parities of the number of occupied Kramer pairs.

For the C_4-symmetric TBC (*3*), the occupied irrep multiplicities m' at $\lambda = i$ are determined by the multiplicities m at $\lambda = 1$ as $m'(A) = m(^1E)$, $m'(B) = m(^2E)$, $m'(^1E) = m(B)$, and $m'(^2E) = m(A)$. The changes of irreps in the evolution $\lambda = 1 \to i$ are $\Delta m(A) = m'(A) - m(A) = m(^1E) - m(A) = \delta_1$, $\Delta m(B) = \delta_1 - \delta_2$, $\Delta m(^1E) = \delta_2 - \delta_1$, and $\Delta m(^2E) = -\delta_1$. Therefore, there will be $|\delta_1|$ crossings formed by A and ^2E and $|\delta_2 - \delta_1|$ crossings formed by B and ^1E. This and the similar analysis for C_2 and TRS-symmetric TBCs are given in Tables 3 and 4 and expanded in (*27*). Our model ($\delta_1 = -1$ and $\delta_2 = 0$) has two level crossings protected by C_2 in the process $\lambda = 1 \to -1$.

The RSI can be calculated either from the momentum space irreps of the band structure or from symmetry-center PG-respecting disordered configurations. In (*27*), we develop a general framework to calculate the RSIs from momentum space irreps and obtain the expressions of RSIs in all wallpaper groups [table S5 (*27*)]. Here we give the expressions for RSIs of wallpaper group $p4$. $p4$ has two inequivalent C_4 Wyckoff positions, a and b, and one C_2 Wyckoff position, c (Fig. 1). PG 4 has two RSIs, δ_1 and δ_2 (Eq. 4), and PG 2 has a single RSI, $\delta_1 = m(B) - m(A)$ [table S2 (*27*)]. The band structure expressions are

$$\delta_{a1} = -m(\Gamma_1) - \frac{m(\Gamma_2)}{2} - m(\Gamma_3\Gamma_4) + \frac{m(\mathrm{M}_2)}{2} + m(\mathrm{M}_3\mathrm{M}_4) + \frac{m(\mathrm{X}_2)}{2} \quad (5)$$

$$\delta_{a2} = -m(\Gamma_1) - m(\Gamma_3\Gamma_4) + m(\mathrm{M}_2) + m(\mathrm{M}_3\mathrm{M}_4) \quad (6)$$

$$\delta_{b1} = \frac{1}{2}m(\Gamma_2) + m(\Gamma_3\Gamma_4) - \frac{1}{2}m(\mathrm{M}_2) - \frac{1}{2}m(\mathrm{X}_2) \quad (7)$$

$$\delta_{b2} = m(\Gamma_2) + m(\Gamma_3\Gamma_4) - m(\mathrm{M}_2) - m(\mathrm{M}_3\mathrm{M}_4) \quad (8)$$

$$\delta_{c1} = m(\Gamma_3\Gamma_4) - m(\mathrm{M}_3\mathrm{M}_4) \quad (9)$$

One can immediately verify that the band structure shown in Fig. 2B has the RSIs $\delta_{a1} = -1$, $\delta_{a2} = 0$ at the a position, which are the same as the results calculated from the disordered configuration.

We find that the RSIs fully describe eigenvalue band topology: EFP is diagnosed by inequalities or mod-equations of RSIs (*15*), and stable topology is diagnosed by fractional RSIs. We prove this in all the wallpaper groups in (*27*). For the wallpaper group $p4$, the stable topology is diagnosed by fractional δ_{a1} and δ_{b1}, which imply topological semimetal phase with Dirac nodes at general momenta (*30*). The fragile topology, by contrast, is diagnosed by the inequality

$$N < \max(2|\delta_{a1}| + \delta_{a2}, 2\delta_{a1} - 3\delta_{a2}) + \max(2|\delta_{b1}| + \delta_{b2}, 2\delta_{b1} - 3\delta_{b2}) + |\delta_{c1}| \quad (10)$$

where N is the number of bands. When this inequality is fullfilled, the RSIs and band number are not consistent with any Wannierizable

Table 2. The RSI groups of 2D PGs.

SOC	TRS	2	*m*	2*mm*	4	4*mm*	3	3*m*	6	6*mm*
✗	✗	$\mathbb{Z}$	$\mathbb{Z}$	$\mathbb{Z}$	$\mathbb{Z}^3$	$\mathbb{Z}^2$	$\mathbb{Z}^2$	$\mathbb{Z}$	$\mathbb{Z}^5$	$\mathbb{Z}^3$
✗	√	$\mathbb{Z}$	$\mathbb{Z}$	$\mathbb{Z}$	$\mathbb{Z}^2$	$\mathbb{Z}$	$\mathbb{Z}$	$\mathbb{Z}$	$\mathbb{Z}^3$	$\mathbb{Z}^3$
√	✗	$\mathbb{Z}$	$\mathbb{Z}$	$\mathbb{Z}_1$	$\mathbb{Z}^3$	$\mathbb{Z}$	$\mathbb{Z}^2$	$\mathbb{Z}$	$\mathbb{Z}^5$	$\mathbb{Z}^2$
√	√	$\mathbb{Z}_2$	$\mathbb{Z}_2$	$\mathbb{Z}_2$	$\mathbb{Z}_2 \times \mathbb{Z}$	$\mathbb{Z}_2 \times \mathbb{Z}$	$\mathbb{Z}$	$\mathbb{Z}$	$\mathbb{Z}_2 \times \mathbb{Z}^2$	$\mathbb{Z}_2 \times \mathbb{Z}^2$

Table 3.

$C_4 : \lambda$	$1 \to i$
$\Delta m(A)$	δ_1
$\Delta m(^1E)$	$\delta_2 - \delta_1$
$\Delta m(B)$	$\delta_1 - \delta_2$
$\Delta m(^2E)$	$-\delta_1$

Table 4.

$C_2 \in \mathbb{R}$	$1 \to -1$
$\Delta m(A)$	$2\delta_1 - \delta_2$
$\Delta m(B)$	$-2\delta_1 + \delta_2$

Corrected 30 March 2020. See full text.

state. One can verify that the band structure shown in Fig. 2B satisfies this inequality and hence has a fragile topology. [See (*27*) for details of the stable and fragile criteria in *p*4.]

Metamaterial systems (*31*, *32*) are the ideal platforms where TBCs can be mechanically tuned. We imagine that Eq. 1 is a Hamiltonian of a mechanical system consisting of mass points connected by rigid bonds or springs. The TBCs of Fig. 2D can be realized by tuning the springs connecting mass points in part I and II from their original values to zero, mimicking $\lambda = 1$ to $\lambda = 0$. The gap between the fragile bands and the other bands must close during this process.

In addition to diagnosing the stable and fragile topological phases, the RSI provides a framework to understand and compute the electronic properties of topologically trivial materials. Many Wannier function–related physical quantities, such as electric or magnetic polarization and multipole, and their responses under external fields, can be qualitatively determined by RSIs. We leave detailed discussions to future studies.

REFERENCES AND NOTES

1. B. Bradlyn *et al.*, *Nature* **547**, 298–305 (2017).
2. J. Cano *et al.*, *Phys. Rev. B* **97**, 035139 (2018).
3. H. C. Po, A. Vishwanath, H. Watanabe, *Nat. Commun.* **8**, 50 (2017).
4. J. Kruthoff, J. de Boer, J. van Wezel, C. L. Kane, R.-J. Slager, *Phys. Rev. X* **7**, 041069 (2017).
5. M. G. Vergniory *et al.*, *Nature* **566**, 480–485 (2019).
6. T. Zhang *et al.*, *Nature* **566**, 475–479 (2019).
7. F. Tang, H. C. Po, A. Vishwanath, X. Wan, *Nature* **566**, 486–489 (2019).
8. W. A. Benalcazar, B. A. Bernevig, T. L. Hughes, *Science* **357**, 61–66 (2017).
9. F. Schindler *et al.*, *Sci. Adv.* **4**, eaat0346 (2018).
10. J. Langbehn, Y. Peng, L. Trifunovic, F. von Oppen, P. W. Brouwer, *Phys. Rev. Lett.* **119**, 246401 (2017).
11. Z. Song, Z. Fang, C. Fang, *Phys. Rev. Lett.* **119**, 246402 (2017).
12. H. C. Po, H. Watanabe, A. Vishwanath, *Phys. Rev. Lett.* **121**, 126402 (2018).
13. J. Cano *et al.*, *Phys. Rev. Lett.* **120**, 266401 (2018).
14. A. Alexandradinata, J. Höller, C. Wang, H. Cheng, L. Lu, arXiv:1908.08541 [cond-mat.str-el] (2019).
15. Z. Song, L. Elcoro, N. Regnault, B. A. Bernevig, arXiv:1905.03262 [cond-mat.mes-hall] (2019).
16. Y. Hwang, J. Ahn, B.-J. Yang, arXiv:1905.08128 [cond-mat.mes-hall] (2019).
17. H. C. Po, L. Zou, T. Senthil, A. Vishwanath, Faithful tight-binding models and fragile topology of magic-angle bilayer graphene. arXiv:1808.02482 [cond-mat] (2018).
18. Z. Song *et al.*, *Phys. Rev. Lett.* **123**, 036401 (2019).
19. R. Bistritzer, A. H. MacDonald, *Proc. Natl. Acad. Sci. U.S.A.* **108**, 12233–12237 (2011).
20. Q. Niu, D. J. Thouless, Y.-S. Wu, *Phys. Rev. B Condens. Matter* **31**, 3372–3377 (1985).
21. X.-L. Qi, Y.-S. Wu, S.-C. Zhang, *Phys. Rev. B Condens. Matter Mater. Phys.* **74**, 045125 (2006).
22. G. van Miert, C. Ortix, *Phys. Rev. B* **98**, 081110 (2018).
23. I. Mondragon-Shem, T. L. Hughes, arXiv:1906.11847 [cond-mat.dis-nn] (2019).
24. H. Song, S.-J. Huang, L. Fu, M. Hermele, *Phys. Rev. X* **7**, 011020 (2017).
25. H. Isobe, L. Fu, *Phys. Rev. B Condens. Matter Mater. Phys.* **92**, 081304 (2015).
26. I. C. Fulga, N. Avraham, H. Beidenkopf, A. Stern, *Phys. Rev. B* **94**, 125405 (2016).
27. Additional analyses are available as supplementary materials.
28. L. Elcoro *et al.*, *J. Appl. Cryst.* **50**, 1457–1477 (2017).
29. B. Bradlyn, Z. Wang, J. Cano, B. A. Bernevig, *Phys. Rev. B* **99**, 045140 (2019).
30. Z. Song, T. Zhang, C. Fang, *Phys. Rev. X* **8**, 031069 (2018).
31. C. Kane, T. Lubensky, *Nat. Phys.* **10**, 39–45 (2014).
32. R. Süsstrunk, S. D. Huber, *Science* **349**, 47–50 (2015).

ACKNOWLEDGMENTS

We are grateful to B. Bradlyn, J. Cano, E. Prodan, and N. Regnault for an earlier initial collaboration on the subject and to B. Lian for helpful discussions. **Funding:** Z.-D.S. and B.A.B. are supported by the U.S. Department of Energy (grant no. DE-SC0016239), the National Science Foundation (EAGER grant no. DMR 1643312), Simons Investigator awards (grant no. 404513), ONR (grant no. N00014-14-1-0330), NSF-MRSEC (grant no. DMR-142051), the Packard Foundation, the Schmidt Fund for Innovative Research, and the Guggenheim Fellowship. L.E. is supported by the Government of the Basque Country (project IT1301-19). The theoretical discovery of the single-group RSI part of the work in the paper was supported by Department of Energy grant no. DE-SC0016239. **Author contributions:** B.A.B. conceived the project, B.A.B. and Z.-D.S. contributed to the ideas of TBC and RSI, and Z.-D.S. and L.E. obtained the RSIs and the fragile criteria. All authors contributed to the writing of the manuscript. **Competing interests:** The authors declare that they have no competing interests. **Data and materials availability:** All data needed to evaluate the conclusions in the paper are present in the paper and/or the supplementary materials.

SUPPLEMENTARY MATERIALS

science.sciencemag.org/content/367/6479/794/suppl/DC1
Supplementary Text S1 to S6
Figs. S1 to S6
Tables S1 to S7

7 October 2019; accepted 17 January 2020
10.1126/science.aaz7650

Twisted bulk-boundary correspondence of fragile topology

Zhi-Da Song, Luis Elcoro and B. Andrei Bernevig

Science **367** (6479), 794-797.
DOI: 10.1126/science.aaz7650

Understanding fragile topology

Exploiting topological features in materials is being pursued as a route to build in robustness of particular properties. Stemming from crystalline symmetries, such topological protection renders the properties robust against defects and provides a platform of rich physics to be studied. Recent developments have revealed the existence of so-called fragile topological phases, where the means of classification due to symmetry is unclear. Z.-D. Song *et al.* and Peri *et al.* present a combined theoretical and experimental approach to identify, classify, and measure the properties of fragile topological phases. By invoking twisted boundary conditions, they are able to describe the properties of fragile topological states and verify the expected experimental signature in an acoustic crystal. Understanding how fragile topology arises could be used to develop new materials with exotic properties.

Science, this issue p. 794, p. 797